Postprint of: Malikan, M.; Uglov, N. S.; Eremeyev, V. A. On instabilities and post-buckling of piezomagnetic and flexomagnetic nanostructures. INTERNATIONAL JOURNAL OF ENGINEERING SCIENCE Vol. 157 (2020), 103395 DOI: 10.1016/j.ijengsci.2020.103395

© 2020. This manuscript version is made available under the CC-BY-NC-ND 4.0 license
http://creativecommons.org/licenses/by-nc-nd/4.0/

On instabilities and post-buckling of piezomagnetic and flexomagnetic nanostructures

Mohammad Malikan[1], Nikolay S. Uglov[2], Victor A. Eremeyev[1,2]*

[1] Department of Mechanics of Materials and Structures,
Gdansk University of Technology, ul. Gabriela Narutowicza 11/12, Gdansk 80-233,
Gdansk, Poland,

[2] R.E. Alekseev Nizhny Novgorod Technical University,
Minin St., 24, Nizhny Novgorod 603950, Russia

*Corresponding author:
Email: mohammad.malikan@pg.edu.pl, nikolay-uglov@mail.ru,
eremeyev.victor@gmail.com

Abstract

We focus on the mechanical strength of piezomagnetic beam-like nanosize sensors during post-buckling. An effective flexomagnetic property is also taken into account. The modelled sensor is selected to be a Euler-Bernoulli type beam. Long-range interactions between atoms result in a mathematical model based on the nonlocal strain gradient elasticity approach (NSGT). Due to possible large deformations within a post-buckling phenomenon, the resultant equations are essentially nonlinear. We establish the results using an analytical approach, including a variety of boundary conditions. We visualize the effective response of the designed sensor for several key components. It was obtained that the flexomagnetic effect is meaningful for less flexible boundary conditions. Besides, it was found that the failure originated from post-buckling occurs sooner if the numerical amounts of nonlocal parameter and the strain gradient one are respectively so small and exceedingly large.

Keywords: Piezomagnetic beam; Post-buckling; Flexomagneticity; Beam-like sensor; Nonlocal elasticity

Symbols

H_z	Magnetic field component	W	Works done by external objects
η_{xxz}	Gradient of the elastic strain	u_1	Cartesian displacements along x axis
σ_{xx}	Stress component	u_3	Cartesian displacements along z axis
ε_{xx}	Strain component	L	Length of the beam
ξ_{xxz}	Hyper stress	h	Thickness of the beam
B_z	Magnetic flux component	u	Axial displacement of the midplane
C_{11}	Elasticity modulus	w	Transverse displacement of the midplane
M_x	Moment stress resultant	z	Thickness coordinate
T_{xxz}	Hyper stress resultant	q_{31}	Component of the third-order piezomagnetic tensor
U	Strain energy	g_{31}	Component the sixth-order gradient elasticity tensor
δ	Symbol of variations	f_{31}	Fourth order flexomagnetic component
N_x	Axial stress resultant	a_{33}	Component of the second-order magnetic permeability tensor
Ψ	Magnetic potential	N_x^0	Initial total in-plane axial force
I_z	Area moment of inertia	ψ	Initial magnetic potential
μ	Nonlocal parameter (nm^2)	A	Area of cross-section of the beam
l	Strain gradient parameter (nm)	N^p	Post-buckling load
Y	Residue in the solution method		
C_1	A constant		
C_2	Integration constant		

1 Introduction

Post-buckling and collapsing behavior are critical to the design of thin structures (Timoshenko & Gere, 1989, Falzon & Aliabadi, 2008, Amabili, 2008, Stevens et al., 1995, Eltaher et al., 2019). Sensitive and certain industrial parts should sustain maximum loads and should be such as to prevent instability and unwanted buckling to avoid large deformations and collapsing. Post-buckling means the deformation of the structure after the start of buckling (bifurcation point), which helps to better understand the failure resistance of the structure after

MOST WIEDZY Downloaded from mostwiedzy.pl

the amount of unauthorized and unallowable in-plane loading. The behavior of post-buckling is a nonlinear one that occurs in a very short time. Also, self-contact may occur during post-buckling due to the high deformation amount. The initial onset of buckling is related to the modes obtained from the modal frequency analysis of the structure. After bifurcation point, the structure has become to confront with a new pattern of deformation, that is a large deformation which buckling load at this time refers to failure of structure. Basically, bifurcation buckling cannot imply collapsing in the structure.

Recently the interest grows to electro- and magnetorheological materials including such coupling higher-order phenomena as flexoelectricity and flexomagneticity, see, e.g. (Basutskar, 2019, Ghayesh and Farajpour, 2019, Ghayesh and Farokhi, 2020, Eremeyev et al., 2020, Espinosa-Almeyda et al., 2020, Mawassy et al., 2020) and the references therein. In particular, magnetic nanoparticles (MNPs) have attracted the attention of many researchers due to their exclusive features (Freitas et al., 2007, Justino et al., 2010, Reddy et al., 2012, Xu and Wang, 2012, Agrawal et al., 2014). Numerous applications are expected for MNPs based on fabricating and developing biosensors. Some of these applications can be stated as biology, clinics, foods, and environments sensors. MNPs can be involved in any substances that are excited by an outer magnetic potential, for example transducers. MNPs are classified into two main categories, paramagnetic and ferromagnetic. Their distinguishing feature appears after the removal of the external magnetic field. Thus, there is no magnetic property in paramagnetic particles after removing the outer magnetic field, while the magnetic property is preserved in ferromagnetic materials.

In the group of MNPs and spinel ferrites, cobalt-ferrite magnetic nanostructures (CFMNs) with chemical symbol $CoFe_4O_2$ have highlighted the significant studies and technological applications. The number of published papers on cobalt-ferrite magnetic

MOST WIEDZY Downloaded from mostwiedzy.pl

nanostructures have been unprecedented during last two decades (Arvand & Hassannezhad, 2014, Theres Baby & Ramaprabhu, 2010; Xin et al., 2013). Of applications of this kind of MNPs are in using electronic devices, optical and magnetic storage in light of its extraordinary features, such as high electromagnetic performance, mechanical hardness, chemical stability, coercivity and high saturation magnetization (Eliseev et al., 2009, Fahrner, 2005, Ju et al., 2008). It should be borne in mind that the CFMNs structure is in the group of ferromagnetic materials. Electromagnetic coupling may influence on the instabilities of such rheological materials, see, e.g., (Broderick et al., 2020, Jalaei and Civalek, 2019, Malikan et al., 2020).

Compared to piezomagneticity (PM), flexomagneticity (FM) is a pervasive property with less restrictive structural symmetry and therefore expands the choice of materials that can be used for sensors and electromechanical actuators (Eliseev et al., 2019, Kabychenkov & Lisovskii, 2019, Lukashev & Sabirianov, 2010, Moosavi et al., 2017, Pereira et al., 2012, Zhang et al., 2012, Zhou et al., 2014). Reduced dimensions would result in larger gradients. This means that the strain difference at a small distance leads to a larger strain gradient. In MNPs technology, the small length scale is discussed, and therefore this type of material will increase the effect of FM, which may even be competitive with PM. This issue is growing rapidly due to the new developments and progresses that have taken place in recent years, especially at the nanoscale.

First, a brief introduction to the first theoretical research on the mechanical response of FM nanostructures is given. Theoretical research performed in the field of FM to elementary papers by Sidhardh & Ray, (2018) and Zhang, Zhang & Chen, (2019). These two early works studied FM in CFMNs within the analysis of static bending deformation. Both research works utilized small deformations and the corresponding domain was assumed as Euler-Bernoulli beam. In these papers, the results were demonstrated on the basis of both direct and converse

MOST WIEDZY Downloaded from mostwiedzy.pl

magnetization effects. The acting static load imposed on the vertical alignment of the domain was uniformly applied. The superiority of the second research against the former one can be presenting several boundary conditions in the study. However, both research studies didn't show perfectly size-dependent influences. Although the surface effect was examined, the nonlocality as a prominent and well-known impact in nanoscale was not evaluated. Recently, Malikan & Eremeyev, (2020a) explored linear frequency behavior of CFMNs on the basis of Euler-Bernoulli type beam. The stress-driven nonlocal elasticity was substituted in the mathematics formulation in order to survey the size-dependent impacts. Their numerical outcomes affirm the behavior of FM is size-dependent. In a nonlinear investigation, Malikan & Eremeyev, (2020b) inspected nonlinear frequency response of CFMNs containing FM effect. To survey the size-dependent influences, they implemented the well-worked nonlocal strain gradient elasticity theory in the mathematical modeling process. Continuing the reported research performed on CFMNs involving FM, we have tried to analyze the post-stability state of the CFMNs in what follows with FM impact. In accordance with the large deformation which occurs in post-buckling conditions, the nonlinear strains of Lagrangian are mixed with Euler-Bernoulli kinematic field which leads to a local constitutive equation. This equation is changed into a nonlocal post-buckling relationship based on the characteristic equation of the nonlocal strain gradient model. Theoretically, four boundary conditions have been estimated, that is, the beam-like sensor with pivot-pivot, fully fixed, pivot-fixed, and fixed-free ends. The assessment is associated with two cases of the sensor, the first one is considered having only PM property and the second one consists of FM with apparent PM. Besides, two states of buckling are investigated, the bifurcation point and its post-time. Later, by variations in fundamental parameters which are vital factors in designing sensors, we measure their influences on the basis of sketched graphical figures.

MOST WIEDZY Downloaded from mostwiedzy.pl

The paper is organized as follows; by means of Section 2 we present the mathematical modelling process of the analysis. Thereafter, Section 3 is associated with the solution methodology. Afterwards, Section 4 of the article considers a preliminary validation by reducing the model into a simple one. Later, Section 5 comes to exhibit a parametric study in order to investigate different factors applicable to affect mechanical behavior of the smart sensor. Finally, by assistance of the conclusion section, we briefly survey the present paper.

2 Mathematical statement

2.1 Basic formulation of structures involving PM and FM

In continue with (Kabychenkov & Lisovskii, 2019, Eliseev et al., 2009, Lukashev & Sabirianov, 2010), the elasticity relations which govern the PM-FM structures would be introduced in what follows. The deformations are restricted to the infinitesimal ones on the basis of early isothermal. Thus, vector-values variables can be magnetic field **H** and displacements *u* as follows (**H** is a first-order tensor)

$$\mathbf{u}=\mathbf{u}(\mathbf{x}),\mathbf{H}=\mathbf{H}(\mathbf{x}) \tag{1}$$

in which $\mathbf{x}$ denotes a position vector. The free energy density *U* based on the PM-FM can be written in the below form

$$U=U(\boldsymbol{\varepsilon},\boldsymbol{\eta},\mathbf{H})=-\frac{1}{2}\mathbf{H}\cdot\mathbf{a}\cdot\mathbf{H}+\frac{1}{2}\boldsymbol{\varepsilon}:\mathbf{C}:\boldsymbol{\varepsilon}+\frac{1}{2}\boldsymbol{\eta}\vdots\mathbf{g}\vdots\boldsymbol{\eta}+\boldsymbol{\varepsilon}:\mathbf{r}\vdots\boldsymbol{\eta} \\ -\mathbf{H}\cdot\mathbf{q}:\boldsymbol{\varepsilon}-\mathbf{H}\cdot\mathbf{f}\vdots\boldsymbol{\eta} \tag{2}$$

in which the strain tensor is defined by $\boldsymbol{\varepsilon}$. Moreover, the gradient of the strain tensor can be presented as below

$$\boldsymbol{\varepsilon}=\frac{1}{2}\left(\nabla\mathbf{u}+\nabla\mathbf{u}^{T}\right),\ \boldsymbol{\eta}=\nabla\boldsymbol{\varepsilon} \tag{3}$$

∇ interprets the 3D nabla-operator. Different tensors are introduced by Eq. (2) for material

MOST WIEDZY Downloaded from mostwiedzy.pl

characterisitcs. Among the mentioned tensors; **f** is the fourth-order flexomagnetic tensor, **C** is the fourth-order elasticity coefficient tensor, the strain and strain-gradient tensors are coupled by **r** that itself is a fifth-order tensor, **g** is the sixth-order gradient elasticity tensor, **a** is the second-order magnetic permeability tensor, **q** is the third-order piezomagnetic tensor, and in addition, "·", ":", and "⋮" define scalar (inner) products in spaces of vectors, second-order and third-order tensors, respectively.

We will now present the relation between **H** through the magnetic potential ψ,

$$\mathbf{H} = -\nabla\psi \tag{4}$$

Static model of flexomagneticity is derived on the basis of principle of virtual work as

$$\delta\Pi = \delta A \tag{5}$$

where $\Pi = \int_V U dV$, and V is the volume of the domain occupying the flexomagnetic structure and δA expresses the work done by outer loads.

To make the process simpler, a simple form is assumed as below

$$\delta A = \int_V \mathbf{F}\cdot\delta\mathbf{u} + \int_{\partial V} \mathbf{t}\cdot\delta\mathbf{u} ds \tag{6}$$

in which **t** and **F** illustrate surface traction and external forces.

On the basis of the standard form of calculus of variations and regarding Eq. (5), one can get

$$\nabla\cdot\left(\boldsymbol{\sigma} - \nabla\cdot\boldsymbol{\xi}\right) + \mathbf{F} = \mathbf{0} \tag{7a}$$

$$\nabla\cdot\mathbf{B} = 0 \tag{7b}$$

where **B** denotes the vector of magnetic induction.

Hence, we introduce the following constitutive equations

$$\boldsymbol{\sigma} = \frac{\partial U}{\partial \boldsymbol{\varepsilon}} \equiv \mathbf{C} : \boldsymbol{\varepsilon} + \mathbf{r} \vdots \boldsymbol{\eta} - \mathbf{H}\cdot\mathbf{q} \tag{8a}$$

MOST WIEDZY Downloaded from mostwiedzy.pl

$$\boldsymbol{\xi} = \frac{\partial U}{\partial \boldsymbol{\eta}} \equiv \mathbf{g} : \boldsymbol{\eta} + \boldsymbol{\varepsilon} : \mathbf{r} - \mathbf{H} \cdot \mathbf{f} \tag{8b}$$

$$\mathbf{B} = -\frac{\partial U}{\partial \mathbf{H}} = \mathbf{a} \cdot \mathbf{H} + \mathbf{q} : \boldsymbol{\varepsilon} + \mathbf{f} \vdots \boldsymbol{\eta} \tag{8c}$$

In what follows we consuider one-dimensional counterparts of these constitutive relations.

2.2 The PM-FM beam-like sensor model

The presented figures determine the physical conditions of the problem in mathematical definitions. Respectively, Figures 1, 2, and 3, display a fully fixed, fully pivot and cantilever beam-like smart sensor with both ends clamped-clamped, guided-guided and clamped-free. A magnetic field is perpendicularly applied which ensues an extra axial force. An axial mechanical load works on the beam to convey the post-buckling state. Boundary conditions are mathematically conducted on the figures. All the boundary objects are rigid. And the beam is configured in a square shape.

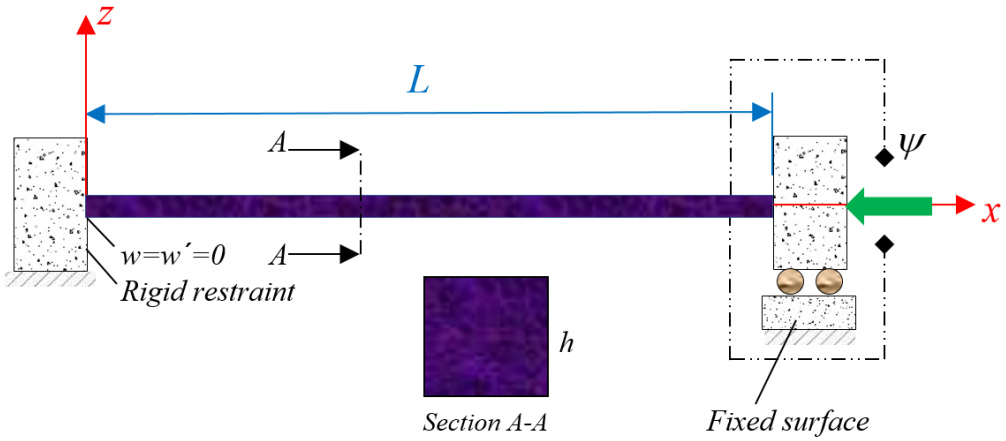

Figure 1. A square beam-like nano sensor containing PM and FM embedded in fully fixed ends

MOST WIEDZY Downloaded from mostwiedzy.pl

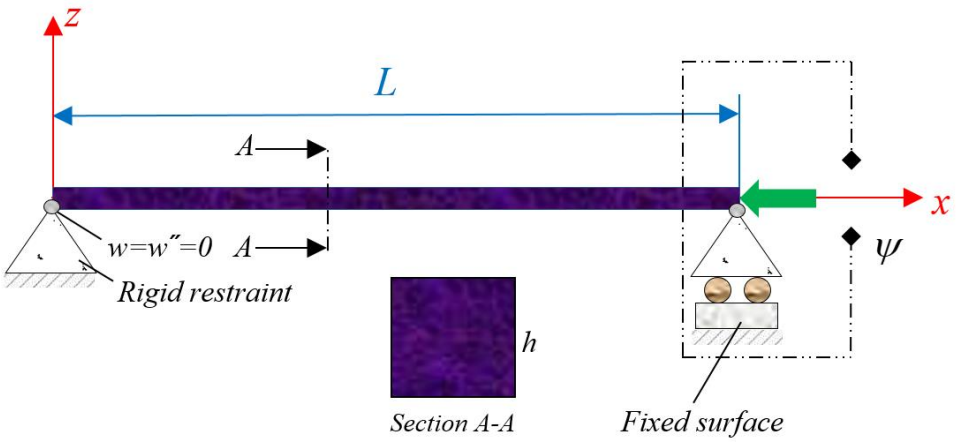

Figure 2. A square beam-like nano sensor containing PM and FM embedded in pivot ends

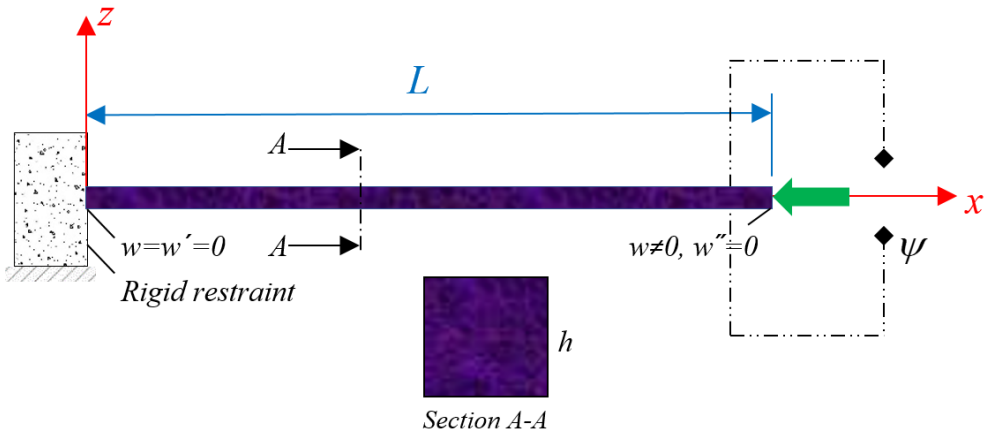

Figure 3. A cantilever square beam-like nano sensor containing PM and FM

It is assumed that the magnetic sensor behaves like a beam structure. Thus, a thin beam approach is carried out as (Hamed et al., 2020, Reddy, 2010, Song & Li, 2007)

$$u_1(x,z) = u(x) - z\frac{dw(x)}{dx} \tag{9}$$

$$u_3(x,z) = w(x) \tag{10}$$

As mentioned before, after buckling and bifurcation point, there would appear the large deformations. Hence, the formulation employs the nonlinear Lagrangian strains as

$$\varepsilon_{xx} = \frac{du}{dx} - z\frac{d^2w}{dx^2} + \frac{1}{2}\left(\frac{dw}{dx}\right)^2 \tag{11}$$

MOST WIEDZY Downloaded from mostwiedzy.pl

$$\eta_{xxz} = \frac{d\varepsilon_{xx}}{dz} = -\frac{d^2 w}{dx^2} \tag{12}$$

To expand the components of stress, hyper stress, and magnetic induction, one can write (Sidhardh & Ray, 2018, Zhang, Zhang & Chen, 2019).

$$\sigma_{xx} = C_{11}\varepsilon_{xx} - q_{31}H_z \tag{13}$$

$$\xi_{xxz} = g_{31}\eta_{xxz} - f_{31}H_z \tag{14}$$

$$B_z = a_{33}H_z + q_{31}\varepsilon_{xx} + f_{31}\eta_{xxz} \tag{15}$$

To derive the characteristics equation, the following variational energy formula based on the Lagrange functional is defined

$$\delta(U - W) = 0 \tag{16}$$

The entire strain energy of the system is established as

$$\delta U = \int_V \left(\sigma_{xx}\delta\varepsilon_{xx} + \xi_{xxz}\delta\eta_{xxz} - B_z\delta H_z\right)dV \tag{17}$$

By computing the above equation, one can obtain the magnetic and mechanical parts of the strain energy as

$$\delta U = \delta\Pi_{U_1}^{Mech} + \delta\Pi_{U_1}^{Mag} + \delta\Pi_{U_2}^{Mech} + \delta\Pi_{U_2}^{Mag} \tag{18}$$

where

$$\delta\Pi_{U_1}^{Mech} = -\int_0^L \left(\frac{dN_x}{dx}\delta u + \frac{d^2M_x}{dx^2}\delta w + \frac{d}{dx}\left(N_x\frac{dw}{dx}\right)\delta w + \frac{d^2T_{xxz}}{dx^2}\delta w\right)dx \tag{19}$$

$$\delta\Pi_{U_1}^{Mag} = -\int_0^L \int_{-h/2}^{h/2} \frac{dB_z}{dz}\delta\Psi dz dx \tag{20}$$

$$\delta\Pi_{U_2}^{Mech} = \left(N_x\delta u - M_x\frac{d\delta w}{dx} - T_{xxz}\frac{d\delta w}{dx} + N_x\frac{dw}{dx}\delta w + \frac{dM_x}{dx}\delta w + \frac{dT_{xxz}}{dx}\delta w\right)\Bigg|_0^L \tag{21}$$

MOST WIEDZY Downloaded from mostwiedzy.pl

$$\delta\Pi_{U_2}^{Mag} = \int_0^L \left(B_z \delta\Psi\right)\Big|_{-h/2}^{h/2} dx \tag{22}$$

Here we introduced the parameters as follows

$$N_x = \int_{-h/2}^{h/2} \sigma_{xx} dz \tag{23}$$

$$M_x = \int_{-h/2}^{h/2} \sigma_{xx} z dz \tag{24}$$

$$T_{xxz} = \int_{-h/2}^{h/2} \xi_{xxz} dz \tag{25}$$

which specify the resultants of stresses on any element of the beam. The external factors, such as magnetic field and mechanical in-plane force, create the work on the system as (Malikan & Eremeyev, 2020c, d)

$$W = -\frac{1}{2}\int_0^L N_x^0 \left(\frac{dw}{dx}\right)^2 dx \tag{26}$$

$$\delta W = -\int_0^L N_x^0 \left(\frac{d\delta w}{dx}\frac{dw}{dx}\right) dx \tag{27}$$

There is a relation between the component of the magnetic field and the magnetic potential as

$$H_z = -\frac{d\Psi}{dz} \tag{28}$$

Assuming the magnetic potential changes along the thickness of the beam and on the basis of converse effect description and closed circuit of the magnetic field, one can present the electrical boundary conditions as

$$\Psi\left(+\frac{h}{2}\right) = \psi, \ \Psi\left(-\frac{h}{2}\right) = 0 \tag{29}$$

Substituting and combining Eqs. (15), (20), (22), (28) and (29) and simplyfying rigorously, one

MOST WIEDZY Downloaded from mostwiedzy.pl

can achieve the magnetic potential and the relevance component as (Sidhardh & Ray, 2018, Zhang, Zhang & Chen, 2019)

$$\Psi = -\frac{q_{31}}{2a_{33}}\left(z^2 - \frac{h^2}{4}\right)\frac{d^2w}{dx^2} + \frac{\psi}{h}\left(z + \frac{h}{2}\right) \tag{30}$$

$$H_z = z\frac{q_{31}}{a_{33}}\frac{d^2w}{dx^2} - \frac{\psi}{h} \tag{31}$$

Consequently, by the help of Eqs. (11), (12), (30), and (31), one can re-write Eqs. (13)-(15) as

$$\sigma_{xx} = C_{11}\left[\frac{du}{dx} + \frac{1}{2}\left(\frac{dw}{dx}\right)^2\right] - z\left(C_{11} + \frac{q_{31}^2}{a_{33}}\right)\frac{d^2w}{dx^2} + \frac{q_{31}\psi}{h} \tag{32}$$

$$\xi_{xxz} = -\left(g_{31} + \frac{q_{31}f_{31}z}{a_{33}}\right)\frac{d^2w}{dx^2} + \frac{f_{31}\psi}{h} \tag{33}$$

$$B_z = q_{31}\left[\frac{du}{dx} + \frac{1}{2}\left(\frac{dw}{dx}\right)^2\right] - f_{31}\frac{d^2w}{dx^2} - \frac{a_{33}\psi}{h} \tag{34}$$

Let us write the local resultants of stresses as

$$N_x = C_{11}A\left[\frac{du}{dx} + \frac{1}{2}\left(\frac{dw}{dx}\right)^2\right] + q_{31}\psi \tag{35}$$

$$M_x = -I_z\left(C_{11} + \frac{q_{31}^2}{a_{33}}\right)\frac{d^2w}{dx^2} \tag{36}$$

$$T_{xxz} = -g_{31}h\frac{d^2w}{dx^2} + f_{31}\psi \tag{37}$$

Eq. (35) plays the role of axial stress resultant which consisted of both mechanical and magnetic terms. Therefore, the magnetic part can be provided as

$$N^{Mag} = q_{31}\psi \tag{38}$$

Then, the total axial loading can be noted as below

$$N_x^0 = N^p + N^{Mag} \tag{39}$$

MOST WIEDZY Downloaded from mostwiedzy.pl

Ultimately the bond of all formulation will lead to local nonlinear equilibrium equations as follows

$$\frac{dN_x}{dx}=0 \tag{40}$$

$$\frac{d^2M_x}{dx^2}+\frac{d^2T_{xxz}}{dx^2}+\frac{d}{dx}\left(N_x\frac{dw}{dx}\right)+N_x^0\frac{d^2w}{dx^2}=0 \tag{41}$$

Size-dependent properties should be established into the mathematical model in order to address nanoscale influences. The size-dependent model is not here restricted to the nonlocal interactions of atoms, but it also considers the higher strain gradients in a constitutive postulate as follows (Lim, Zhang & Reddy, 2015)

$$\left(1-\mu\frac{d^2}{dx^2}\right)\sigma_{xx}^{NonLocal}=\left(1-l^2\frac{d^2}{dx^2}\right)\sigma_{xx}^{Local} \tag{42}$$

where $\mu=(e_0a)^2$. For applications of nonlocal approach to beam models we refer also to (Barretta and de Sciarra, 2019, Barreta et al., 2020).

By developing Eq. (42) for the axial stress of present problem (Eq. (42)), one can see

$$\left(1-\mu\frac{d^2}{dx^2}\right)\sigma_{xx}^{NonLocal}=\left(1-l^2\frac{d^2}{dx^2}\right)\left\{C_{11}\left[\frac{du}{dx}+\frac{1}{2}\left(\frac{dw}{dx}\right)^2\right]-z\left(C_{11}+\frac{q_{31}^2}{a_{33}}\right)\frac{d^2w}{dx^2}+\frac{q_{31}\psi}{h}\right\} \tag{43}$$

By integrating rigorously from both parts of Eq. (43) based on the dz and using Eqs. (23-25), one can express

$$N_x-\mu\frac{d^2N_x}{dx^2}=C_{11}A\left(1-l^2\frac{d^2}{dx^2}\right)\left\{\left[\frac{du}{dx}+\frac{1}{2}\left(\frac{dw}{dx}\right)^2\right]+q_{31}\psi\right\} \tag{44}$$

$$M_x-\mu\frac{d^2M_x}{dx^2}=-I_z\left(C_{11}+\frac{q_{31}^2}{a_{33}}\right)\left(1-l^2\frac{d^2}{dx^2}\right)\left\{\frac{d^2w}{dx^2}\right\} \tag{45}$$

$$T_{xxz}-\mu\frac{d^2T_{xxz}}{dx^2}=\left(1-l^2\frac{d^2}{dx^2}\right)\left\{-g_{31}h\frac{d^2w}{dx^2}+f_{31}\psi\right\} \tag{46}$$

By re-writing Eq. (41) based on the first term and plugging it in Eq. (45), one can have (Karami

MOST WIEDZY Downloaded from mostwiedzy.pl

& Janghorban, 2019, Karami et al., 2020, Karami & Janghorban, 2020, Eyvazian et al., 2020, Li & Hu, 2017, Malikan et al., 2019, Malikan et al., 2020, Malikan et al., 2018, Sahmani & Safaei, 2019, Ebrahimi et al., 2019)

$$M_x = -\mu\left(\frac{d^2T_{xxz}}{dx^2}+\frac{d}{dx}\left(N_x\frac{dw}{dx}\right)+N_x^0\frac{d^2w}{dx^2}\right)-I_z\left(C_{11}+\frac{q_{31}^2}{a_{33}}\right)\left(\frac{d^2w}{dx^2}-l^2\frac{d^4w}{dx^4}\right) \tag{47}$$

Since there are two unknown variables (u and w) in the equations, it would result in difficulties to solve the equations as far as there is a third unknown, which is post-critical buckling load (N^p). Therefore, let us write the u based on the w as

$$N_x = C_{11}A\left[\frac{du}{dx}+\frac{1}{2}\left(\frac{dw}{dx}\right)^2\right]=C_1 \tag{48}$$

Writing Eq. (48) based on the u and integrating gives

$$u = -\frac{1}{2}\int_0^L\left(\frac{dw}{dx}\right)^2dx+\frac{C_1}{C_{11}A}x+C_2 \tag{49}$$

Imposing the initial conditions as $u(0)=u(L)=0$, one can obtain

$$N_x = \frac{C_{11}A}{2L}\int_0^L\left(\frac{dw}{dx}\right)^2dx \tag{50}$$

Thereafter, based on the Eqs. (39), (41), (47), and (50), the model of the problem can be formulated mathematically as a single integro-differential equation

$$\begin{aligned}
&-g_{31}h\frac{d^4w}{dx^4}+\left(N^p+q_{31}\psi\right)\frac{d^2w}{dx^2}-\mu\left(-g_{31}h\frac{d^6w}{dx^6}+\left(N^p+q_{31}\psi\right)\frac{d^4w}{dx^4}\right)\\
&-\mu\left[\frac{C_{11}A}{2L}\int_0^L\left(\frac{dw}{dx}\right)^2dx\right]\frac{d^4w}{dx^4}-\mu\frac{d}{dx}\left[\frac{C_{11}A}{2L}\int_0^L\left(\frac{dw}{dx}\right)^2dx\right]\frac{d^3w}{dx^3}\\
&-\mu\frac{d^2}{dx^2}\left[\frac{C_{11}A}{2L}\int_0^L\left(\frac{dw}{dx}\right)^2dx\right]\frac{d^2w}{dx^2}-\mu\frac{d^3}{dx^3}\left[\frac{C_{11}A}{2L}\int_0^L\left(\frac{dw}{dx}\right)^2dx\right]\frac{dw}{dx}\\
&+\left[\frac{C_{11}A}{2L}\int_0^L\left(\frac{dw}{dx}\right)^2dx\right]\frac{d^2w}{dx^2}+\frac{d}{dx}\left[\frac{C_{11}A}{2L}\int_0^L\left(\frac{dw}{dx}\right)^2dx\right]\frac{dw}{dx}\\
&-I_z\left(C_{11}+\frac{q_{31}^2}{a_{33}}\right)\left(\frac{d^4w}{dx^4}-l^2\frac{d^6w}{dx^6}\right)=0
\end{aligned} \tag{51}$$

MOST WIEDZY Downloaded from mostwiedzy.pl

3 Solution approach

In this section, the aim is to solve the appropriate boundary conditions along with the nonlinear governing equation (Eq. (51)). Some admissible shape functions are described by which several end conditions are satisfied. The procedure is entirely analytical. However, as far as the boundary conditions seem to be homogeneous, the present analytical solution sounds like an exact solving method (Malikan & Eremeyev, 2020e).

$$w(x) = W \cdot X(x) \tag{52}$$

where the deflection resulted from post-buckling conditions is dedicated symbolically by *W*. The permissible shape functions appeared in the following can satisfy quite different end conditions (Malikan & Eremeyev, 2020e, Gunda, 2014). The notations are respectively allocated for guided or pivot (S), fixed or clamped (C) and free (F) border conditions (BCs) as follows

$$\text{SS: } X(x) = \sin\left(\frac{\pi}{L}x\right) \tag{53}$$

$$\text{CC: } X(x) = \sin^2\left(\frac{\pi}{L}x\right) \tag{54}$$

$$\text{CS: } \begin{array}{c} X(x) = \delta_1\left(\sin(k_1 x) - \mathrm{k}_1 L\cos(k_1 x) + k_1 L\left(1-(x/L)\right)\right) \\ \delta_1 = 0.1709382933,\ \mathrm{k}_1 = 1.4318\pi/L \end{array} \tag{55}$$

$$\text{CF: } X(x) = \sin\left(\frac{\pi}{4L}x\right)\cos\left(\frac{\pi}{4L}x\right) \tag{56}$$

where for example CF accounts a side with free and another one with fully fixture conditions. Incorporating Eq. (51) with Eq. (52) and integrating over the length of the beam, one attains

$$\left(K_L + K_{NL} - N^p K_G\right) X = 0 \tag{57}$$

MOST WIEDZY Downloaded from mostwiedzy.pl

After some algebra, one obtains the nonlinear algebraic equation that by computing the N^p, that presents post-buckling loads for the magnetic beam-like sensor considering FM. The coefficients in Eq. (57) can be expanded as below

$$K_L = \int_0^L \left[\lambda_1(x) \cdot Y \right] dx \tag{58}$$

$$K_{NL} = \int_0^L \left[\lambda_2(x) \cdot Y \right] dx \tag{59}$$

$$K_G = \int_0^L \left[\lambda_3(x) \cdot Y \right] dx \tag{60}$$

in which Y illustrates a residue, λ_1 to λ_3 are as follows:

$$\begin{aligned} &\lambda_1(x) = -g_{31} h \frac{d^4 w}{dx^4} + q_{31} \psi \frac{d^2 w}{dx^2} - \mu \left(-g_{31} h \frac{d^6 w}{dx^6} + q_{31} \psi \frac{d^4 w}{dx^4} \right) \\ &-I_z \left(C_{11} + \frac{q_{31}^2}{a_{33}} \right) \left(\frac{d^4 w}{dx^4} - l^2 \frac{d^6 w}{dx^6} \right) \end{aligned} \tag{61}$$

$$\begin{aligned} &\lambda_2(x) = -\mu \left[\frac{C_{11} A}{2L} \int_0^L \left(\frac{dw}{dx} \right)^2 dx \right] \frac{d^4 w}{dx^4} - \mu \frac{d}{dx} \left[\frac{C_{11} A}{2L} \int_0^L \left(\frac{dw}{dx} \right)^2 dx \right] \frac{d^3 w}{dx^3} \\ &-\mu \frac{d^2}{dx^2} \left[\frac{C_{11} A}{2L} \int_0^L \left(\frac{dw}{dx} \right)^2 dx \right] \frac{d^2 w}{dx^2} - \mu \frac{d^3}{dx^3} \left[\frac{C_{11} A}{2L} \int_0^L \left(\frac{dw}{dx} \right)^2 dx \right] \frac{dw}{dx} \\ &+ \left[\frac{C_{11} A}{2L} \int_0^L \left(\frac{dw}{dx} \right)^2 dx \right] \frac{d^2 w}{dx^2} + \frac{d}{dx} \left[\frac{C_{11} A}{2L} \int_0^L \left(\frac{dw}{dx} \right)^2 dx \right] \frac{dw}{dx} = 0 \end{aligned} \tag{62}$$

$$\lambda_3(x) = \frac{d^2 w}{dx^2} - \mu \frac{d^4 w}{dx^4} \tag{63}$$

If we assume $K_{NL} = 0$, the bifurcation buckling will result.

MOST WIEDZY Downloaded from mostwiedzy.pl

4 Validity

To begin the discussion and results of the present study, a results comparison is required to verify the analytical solution's efficiency and accuracy. This is performed regarding Tables 1 to 4 (Wang et al., 2006, Pradhan & Reddy, 2011). In the existing data, bifurcation buckling of a common squared section nanoscale beam was investigated on the basis of the following elasticity properties; E=1TPa, υ= 0.19, the exact solution method (Wang et al., 2006) and differential transformed solution method (DTM) (Pradhan & Reddy, 2011). Both references benefited from the Euler-Bernoulli beam. All the boundary conditions examined in the present paper are validated. A reasonable agreement is observed between the present solution and those reported in (Wang et al., 2006, Pradhan & Reddy, 2011).

Table 1. For a SS beam.

	P_{Cr} (nN)								
	μ=0 nm^2			μ=1 nm^2			μ=4 nm^2		
L (nm)	(Wang et al., 2006)	(Pradhan & Reddy, 2011)	Present	(Wang et al., 2006)	(Pradhan & Reddy, 2011)	Present	(Wang et al., 2006)	(Pradhan & Reddy, 2011)	Present
10	4.8447	4.8447	4.84473	4.4095	4.4095	4.40953	3.4735	3.4735	3.47346
12	3.3644	3.3644	3.36439	3.1486	3.1486	3.14859	2.6405	2.6405	2.64049
14	2.4718	2.4718	2.47180	2.3533	2.3533	2.35330	2.0574	2.0574	2.05739
16	1.8925	1.8925	1.89247	1.8222	1.8222	1.82222	1.6396	1.6396	1.63962
18	1.4953	1.4953	1.49529	1.4511	1.4511	1.45109	1.3329	1.3329	1.33288
20	1.2112	1.2112	1.21118	1.182	1.182	1.18201	1.1024	1.1024	1.10238

MOST WIEDZY Downloaded from mostwiedzy.pl

Table 2. For a CS beam.

	P_{Cr} (nN)								
	μ=0 nm^2			μ=1 nm^2			μ=2 nm^2		
L (nm)	(Wang et al., 2006)	(Pradhan & Reddy, 2011)	Present	(Wang et al., 2006)	(Pradhan & Reddy, 2011)	Present	(Wang et al., 2006)	(Pradhan & Reddy, 2011)	Present
10	9.887	9.887	9.91111	8.2295	8.2295	8.24614	7.048	7.048	7.06015
12	6.886	6.886	6.88271	6.0235	6.0235	6.03631	5.3651	5.3651	5.37530
14	5.044	5.044	5.05668	4.5744	4.5744	4.58441	4.1844	4.1844	4.19285
16	3.8621	3.8621	3.87152	3.5804	3.5804	3.58849	3.337	3.337	3.34403
18	3.0516	3.0516	3.05898	2.873	2.873	2.87954	2.7141	2.7141	2.71998
20	2.4718	2.4718	2.47777	2.3533	2.3533	2.35871	2.2456	2.2456	2.25057

Table 3. For a CC beam.

	P_{Cr} (nN)								
	μ=0 nm^2			μ=1 nm^2			μ=2 nm^2		
L (nm)	(Wang et al., 2006)	(Pradhan & Reddy, 2011)	Present	(Wang et al., 2006)	(Pradhan & Reddy, 2011)	Present	(Wang et al., 2006)	(Pradhan & Reddy, 2011)	Present
10	19.379	19.379	19.37895	13.8939	13.8939	13.89386	10.828	10.828	10.8288
12	13.458	13.458	13.45760	10.652	10.652	10.56197	8.6917	8.6917	8.69178
14	9.877	9.877	9.88721	8.2296	8.2296	8.22960	7.0479	7.0479	7.04799
16	7.4699	7.4699	7.56990	6.5585	6.5585	6.55849	5.7854	5.7854	5.78550
18	5.9811	5.9811	5.98115	5.3375	5.3375	5.33153	4.8091	4.8091	4.80918
20	4.8447	4.8447	4.84473	4.4095	4.4095	4.40953	4.046	4.046	4.04607

MOST WIEDZY Downloaded from mostwiedzy.pl

Table 4. For a CF beam.

	P_{Cr} (nN)								
	μ=0 nm^2			μ=1 nm^2			μ=2 nm^2		
L (nm)	(Wang et al., 2006)	(Pradhan & Reddy, 2011)	Present	(Wang et al., 2006)	(Pradhan & Reddy, 2011)	Present	(Wang et al., 2006)	(Pradhan & Reddy, 2011)	Present
10	1.2112	1.2112	1.21118	1.1820	1.1820	1.18201	1.1542	1.1542	1.15422
12	0.8411	0.8411	0.84109	0.8269	0.8269	0.82693	0.8132	0.8132	0.81323
14	0.6179	0.6179	0.61795	0.6103	0.6103	0.61026	0.6027	0.6027	0.60277
16	0.4731	0.4731	0.47311	0.4686	0.4686	0.46860	0.4641	0.4641	0.46417
18	0.3738	0.3738	0.37382	0.3710	0.3710	0.37099	0.3682	0.3682	0.36821
20	0.3028	0.3028	0.30279	0.3009	0.3009	0.30094	0.2991	0.2991	0.29910

5 Discussion and results

After the preliminary comparison, the nonlinear buckling and post-buckling behaviors of a CFMN comprising FM in a parametric study based on some examples are calculated. It is well-established that a CFMN structure gives perceptibly FM effect in a nanosize (Sidhardh & Ray, 2018, Zhang, Zhang & Chen, 2019, Malikan & Eremeyev, 2020a, b). Accordingly, the properties of CFMNs in the framework of magnetic and mechanics are available as (Pan et al. 2003, Pan et al., 2005, Senthil et al., 2018)

Table 5. Magneto-mechanical properties for CFMN beam-like nanosize sensors.

$CoFe_2O_4$
C_{11}=286e9 N/m^2
f_{31}=10^{-9} N/Ampere
q_{31}=580.3 N/Ampere.m
a_{33}=1.57×10^{-4} N/Ampere^2

MOST WIEDZY Downloaded from mostwiedzy.pl

5.1 Size-dependent effects

Due to the existence of two variable parameters in NSGT, their exact amounts are momentous. However, with regard to the literature (Ansari et al., 2010, Akbarzadeh Khorshidi, 2018), their values are dependent on several cases and there cannot be a constant value for each one in association with every nanomaterial.

Figures 4 and 5 focus on the effect of size-dependent parameters on the buckling and post-buckling behaviors of the nanobeam. In the first figure, by assuming the nonlocal parameter to be constant, we evaluate the changes in the strain gradient parameter. All four cases of boundary conditions mentioned before are presented in these figures. It is important to note that the buckling's results obtained linearly are represented by the index (L) and the post-buckling results obtained by nonlinear analysis are displayed by the index (NL). This is true for all diagrams. Moreover, CBL in all diagrams means critical load whether from buckling or post-buckling. The first point that we get to a superficial look at Figure 4 is that the strain gradient parameter has the greatest impact on the beam with the boundary condition of the two sides completely clamped. Interestingly, this effect decreases with an increase in the degree of freedom of border conditions. If we pay attention to Figure 4, this result is quite clear in the behavior of the curves. Thus, the changes in the strain gradient parameter, for example, have completely differentiated the slope of the beam's results with the fully fixed boundary conditions. Another important point that can be obtained by looking more closely at this figure is that by increasing the values of the strain gradient parameter, the buckling and post-buckling results of each boundary condition are converging. This theorem can be interpreted as meaning that at very large values of the strain gradient parameter, the distance between the occurrence of buckling and the failure of the material will be smaller. Therefore, large values of this parameter indicate faster failure of the material. On the other hand, with a brief overview of

MOST WIEDZY Downloaded from mostwiedzy.pl

Figure 5, other points can be extracted. In this figure, in contrast to Figure 4, we assume the strain gradient parameter is constant and examine the changes in the nonlocal parameter. It is quite clear from Figure 5 that increasing the values of the nonlocal parameter decreases the results. However, this decreasing trend in the results of buckling analysis is more regular and with a certain harmony. Also, the severity in the decrease of the results, which is as a result of increasing the nonlocal parameter, in the buckling results is more than the post-buckling ones. In a point of fact, it can be said that the effect of the nonlocal parameter decreases after buckling. Another interesting result is that with increasing the nonlocal parameter, the distance between the curves related to the buckling and post-buckling results increases. Therefore, it can be stated that if the value of the nonlocal parameter is large, it indicates that the material fails later after buckling. As a final point obtained from Figures 4 and 5, it can be stated that the cantilever beam behind the buckle will be extremely weak compared to the other cases. This result can be understood by comparing the difference between the curves of the cantilever beam in the two states of buckling and post-buckling with other boundary conditions.

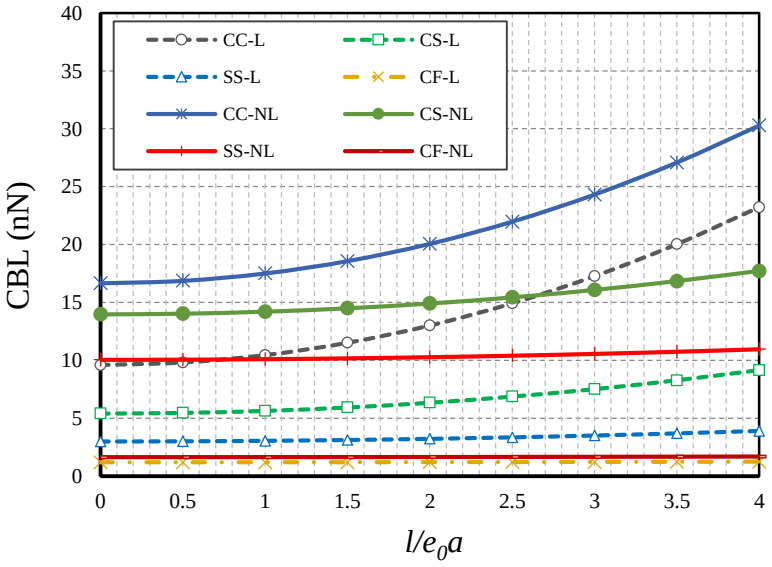

Fig. 4. Size-dependent parameters vs. CBL for different cases of BCs (Ψ=1 mA, e_0a=0.5 nm, L=10h)

MOST WIEDZY Downloaded from mostwiedzy.pl

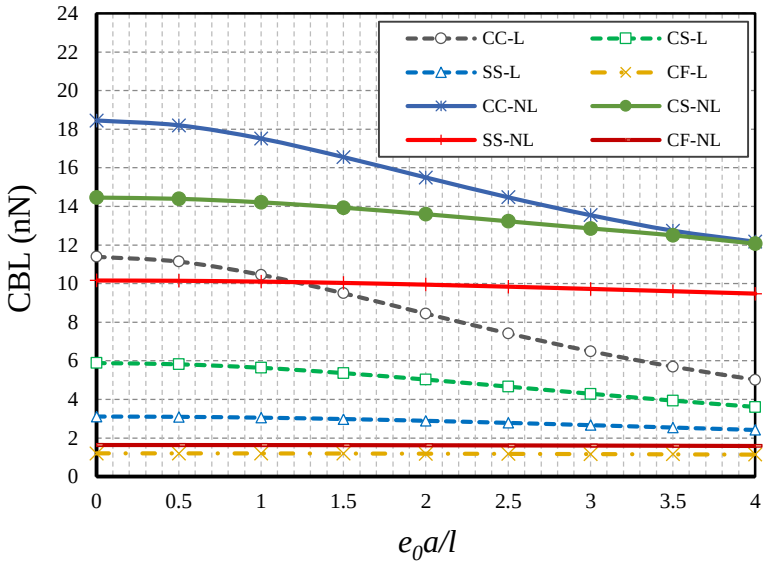

Fig. 5. Size-dependent parameters vs. CBL for different cases of BCs (Ψ=1 mA, l=0.5 nm, L=10h)

5.2 Magnetic field effect

Assuming that a magnetic field surrounds the sensor, changes, and increases or even decreases the magnitude of the magnetic potential can be very important and have a significant impact on the mechanical behavior of the sensor. Hence, we would like to examine this effect with the help of Figure 6. The magnitude of the magnetic potential is considered from negative 2 to positive 2 to include both positive and negative external fields. First, it is interesting to know that increasing the numerical value of the external potential leads to an increase in the stiffness of the material and ultimately its greater stability. As can be seen from the curves, the increasing slope of the results is linear. In addition, the distances between the post-buckling results' curves are longer than the buckling-related curves. This means that the boundary condition becomes more important in the post-buckling mode. On the other hand, the cantilever beam goes into buckling and post-buckling in negative values of external potential with a tensile axial force,

MOST WIEDZY Downloaded from mostwiedzy.pl

which of course other cases will experience, but later than the cantilever beam with a larger negative potential.

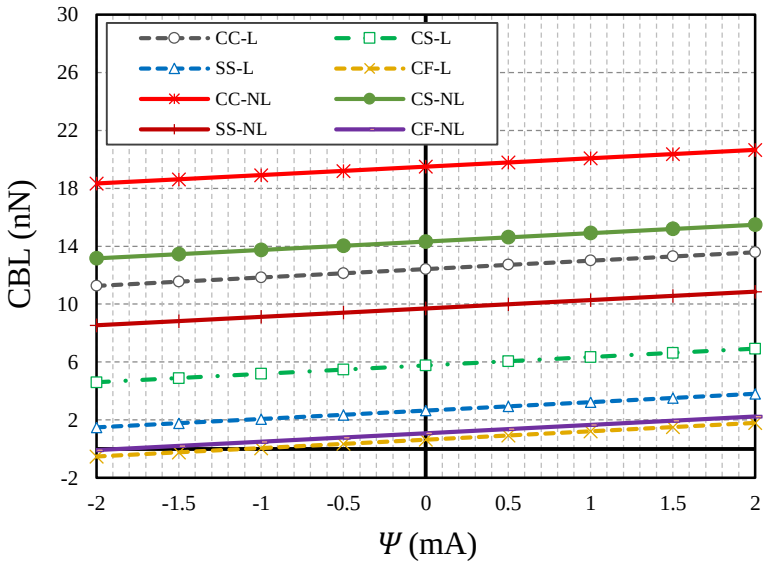

Fig. 6. Magnetic potential vs. CBL for different cases of BCs (l=1 nm, e_0a=0.5 nm, L=10h)

5.3 Slenderness ratio effect

The amount of narrowing of structures in buckling has always been a vital issue in their design. The ratio of length to thickness (slenderness ratio) in the design of beams and plates is a serious parameter for their stability. We will evaluate this for the nanosensor under study using Figures 7 and 8. Figure 7 is plotted for the two boundary conditions CC and SS and Figure 8 is drawn for the two boundary conditions CS and CF. As can be seen from both figures, with increasing the slenderness coefficient of the beam, the results of buckling and post-buckling tend to each other. This means that in beams with long lengths and small thicknesses, the post-buckling state and failure occur in a very short time after buckling. It can even be said that in very long beams, buckling and post-buckling occur together. But if the slenderness coefficient of the beam is low, and it is better to say that if the length of the beam is not long, the material will fail after bifurcation buckling after a certain time, and this is better for the structure. Therefore,

MOST WIEDZY Downloaded from mostwiedzy.pl

in beam-like sensors with long lengths, designers should think of measures to prevent material failure with the occurrence of buckling.

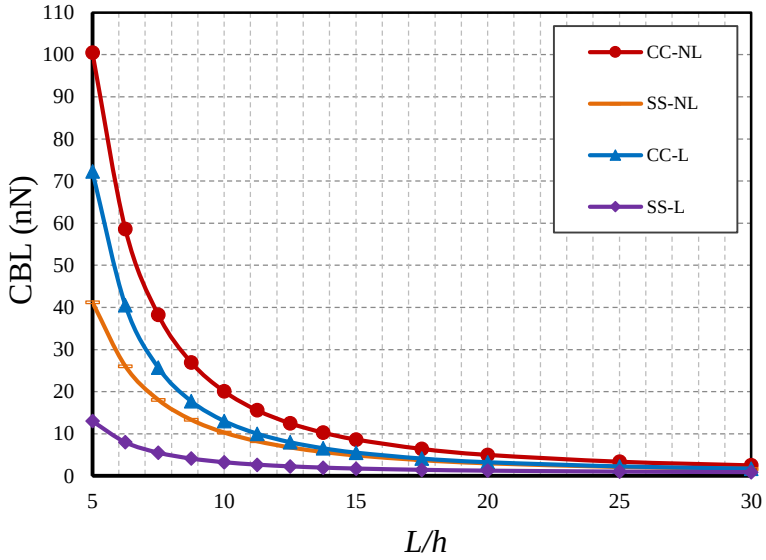

Fig. 7. Slenderness ratio vs. CBL for different BCs (Ψ=1 mA, e_0a=0.5 nm, l=1 nm)

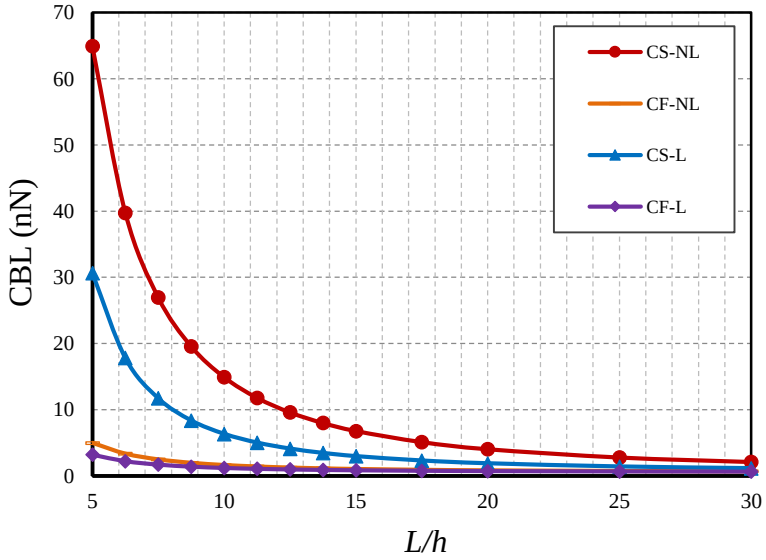

Fig. 8. Slenderness ratio vs. CBL for different BCs (Ψ=1 mA, e_0a=0.5 nm, l=1 nm)

5.4 Flexomagneticity (FM) effect

MOST WIEDZY Downloaded from mostwiedzy.pl

The study of the effect of FM in post-buckling conditions is the main goal of this research. For this purpose, Figures 9 to 12 are drawn. In Figure 9 and the horizontal axis of the diagram, we examine the changes in the nonlocal parameter while the beam is embedded in the two boundary conditions CC and SS. The beam is modeled in two modes without FM effect (PM sensor) and considering this effect (PFM sensor). The same factors, however, are presented for the two boundary conditions CF and CS in Figure 10. Figures 11 and 12 are similar to Figures 9 and 10, but with the difference that the horizontal axis of the diagrams shows the changes in magnetic potential. At the first glance, it can be seen that the flexomagnetic effect is noticeable when the boundary conditions are fully fixed in at least one of the two ends of the beam. It can be seen from the figures that in the CC and CS boundary conditions, the greatest effect can be obtained from the FM influence. On the other hand, the results of buckling and post-buckling load in PFM mode are larger, which indicates that the FM effect in the positive magnetic field leads to greater stability of the material.

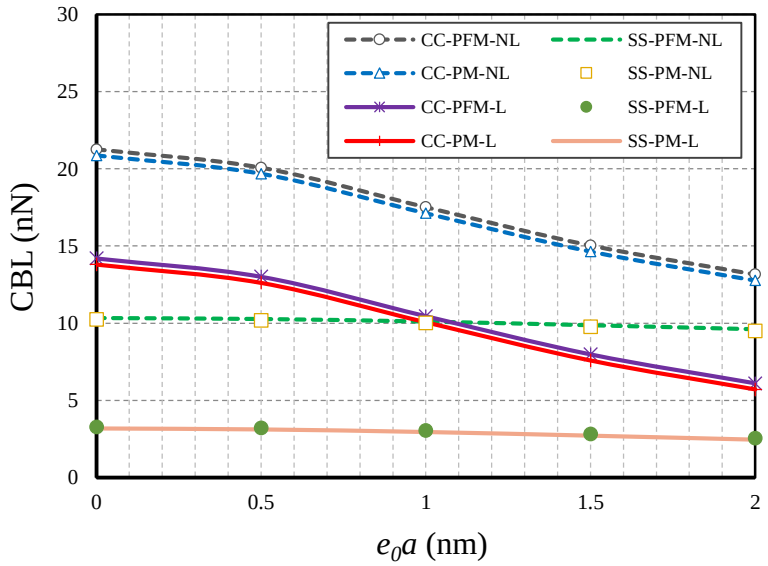

Fig. 9. Nonlocal parameter vs. CBL for different cases of BCs (Ψ=1 mA, l=0.5 nm, L=10h)

MOST WIEDZY Downloaded from mostwiedzy.pl

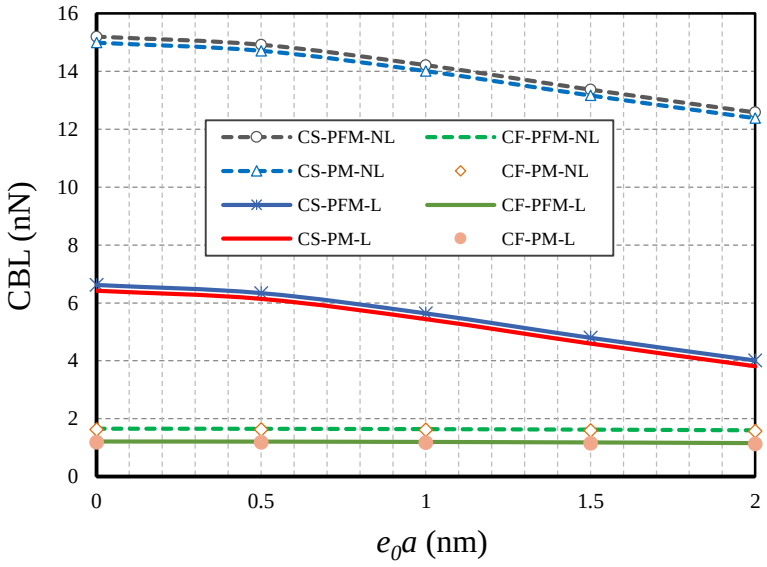

Fig. 10. Nonlocal parameter vs. CBL for different cases of BCs (Ψ=1 mA, l=0.5 nm, L=10h)

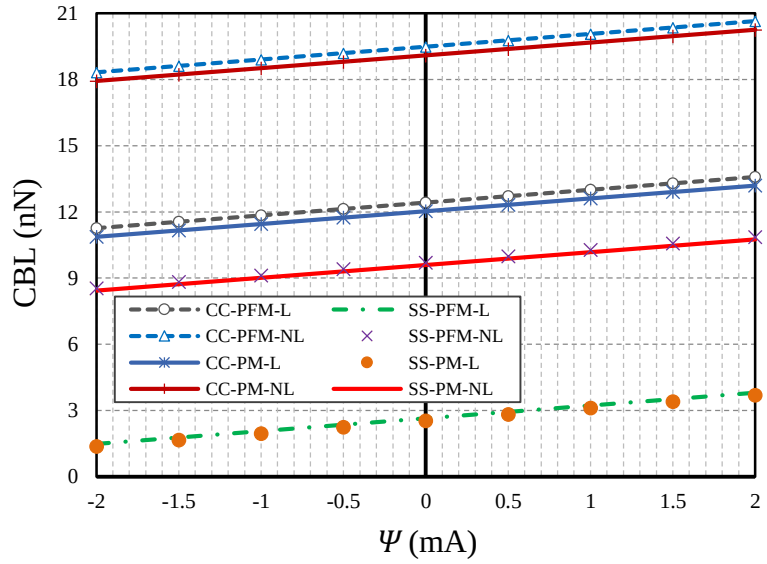

Fig. 11. Magnetic potential vs. CBL for different cases of BCs (l=1 nm, e_0a=0.5 nm, L=10h)

MOST WIEDZY Downloaded from mostwiedzy.pl

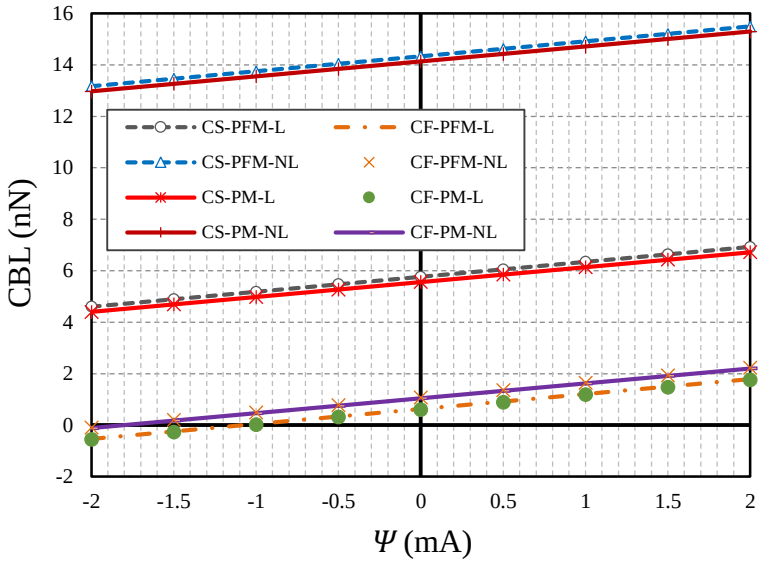

Fig. 12. Magnetic potential vs. CBL for different cases of BCs (l=1 nm, e_0a=0.5 nm, L=10h)

6 Conclusions

Both bifurcation buckling and post-buckling phenomena for cobalt-ferrite magnetic nanostructures (CFMNs) were discussed in this paper while the magnetic nanoparticle (MNP) accommodated flexomagneticity (FM) influence. The mathematical model was derived according to the Euler-Bernoulli beam, nonlinear Lagrangian-von Kármán strains and nonlocal approach of strain gradient elasticity (NSGT). The buckling and post-buckling were analytically studied for changes in size-dependent parameters, slenderness ratio, magnetic field in the presence and absence of the FM when the ends conditions of the beam-like nanosensor were differed. This research work concluded that:

- The post-buckling and failure resulted from it, would happen sooner for nanostructures whilst the values of strain gradient and the nonlocal parameters are respectively very large and negligible.

MOST WIEDZY Downloaded from mostwiedzy.pl

- In post-buckling, both small scale parameters affect remarkably results of boundary conditions with lower degrees of freedom.
- In so-called lengthy sensors, critical buckling and post-buckling loads can occur simultaneously. This means, exactly at the time of critical buckling the structure will fail.
- The boundary condition with lower degrees of freedom makes the flexomagnetic effect more pronounced.

Acknowledgements

V.A.E. and N.S.U. acknowledge the support by grant 14.Z50.31.0036 awarded to R. E. Alekseev Nizhny Novgorod Technical University by Department of Education and Science of the Russian Federation.

References

Agrawal, S., Paknikar, K., & Bodas, D. (2014). Development of immunosensor using magnetic nanoparticles and circular microchannels in PDMS. *Microelectronic Engineering*, *115*, 66-69.

Akbarzadeh Khorshidi, M. (2018). The material length scale parameter used in couple stress theories is not a material constant. *International Journal of Engineering Science*, *133*, 15-25.

Amabili, M. (2008). Nonlinear vibrations and stability of shells and plates. Cambridge University Press.

Ansari, R., Sahmani, S., & Arash, B. (2010). Nonlocal plate model for free vibrations of single-layered graphene sheets. *Physics Letters A*, *375*, 53-62.

Arvand, M., & Hassannezhad, M. (2014). Magnetic core–shell Fe_3O_4@SiO_2/MWCNT nanocomposite modified carbon paste electrode for amplified electrochemical sensing of uric acid. *Materials Science and Engineering*: *C*, *36*, 160-167.

MOST WIEDZY Downloaded from mostwiedzy.pl

Barretta, R., Čanađija, M., de Sciarra, F.M. (2020). On thermomechanics of multilayered beams. *International Journal of Engineering Science*, 155, 103364.

Barretta, R., de Sciarra, F.M. (2019) Variational nonlocal gradient elasticity for nano-beams. *International Journal of Engineering Science*, 143,.73-91.

Basutkar, R., (2019). Analytical modelling of a nanoscale series-connected bimorph piezoelectric energy harvester incorporating the flexoelectric effect. *International Journal of Engineering Science*, 139,.42-61.

Broderick, H.C., Righi, M., Destrade, M., Ogden, R.W. (2020). Stability analysis of charge-controlled soft dielectric plates. *International Journal of Engineering Science,* 151, 103280

Ebrahimi, F., Dabbagh, A., Tornabene, F., & Civalek, O. (2019). Hygro-thermal effects on wave dispersion responses of magnetostrictive sandwich nanoplates. *Advanced Nano Research, 7*, 157-167.

Eliseev, E. A., Morozovska, A. N., Glinchuk, M. D., & Blinc, R. (2009). Spontaneous flexoelectric/flexomagnetic effect in nanoferroics. *Physical Review B, 79*, 165433.

Eliseev, E. A., Morozovska, A. N., Khist, V. V., & Polinger, V. (2019). effective flexoelectric and flexomagnetic response of ferroics, In Recent Advances in Topological Ferroics and their Dynamics, Solid State Physics; Stamps, R. L., Schultheis, H.; Elsevier, Netherlands, *70*, 237-289.

Eltaher, M. A., Mohamed, N., Mohamed, S., & Seddek, L. F. (2019). Postbuckling of Curved Carbon Nanotubes Using Energy Equivalent Model. *Journal of Nano Research, 57*, 136-157.

Eremeyev, V.A., Ganghoffer, J.F., Konopińska-Zmysłowska, V., Uglov, N.S. (2020). Flexoelectricity and apparent piezoelectricity of a pantographic micro-bar. *International Journal of Engineering Science*, 149, 103213.

Espinosa-Almeyda, Y., Camacho-Montes, H., Otero, J.A., Rodríguez-Ramos, R., López-Realpozo, J.C., Guinovart-Díaz, R. and Sabina, F.J. (2020) Interphase effect on the effective magneto-electro-elastic properties for three-phase fiber-reinforced composites by a semi-analytical approach. *International Journal of Engineering Science*, 154, 103310.

MOST WIEDZY Downloaded from mostwiedzy.pl

Eyvazian, A., Shahsavari, D., & Karami, B. (2020). On the dynamic of graphene reinforced nanocomposite cylindrical shells subjected to a moving harmonic load. *International Journal of Engineering Science*, *154*, Article 103339.

Fahrner, W. (2005). Nanotechnology and Nanoelectronics. 1st ed.; Springer, Germany, 269.

Falzon, B. G., & Aliabadi, M. H. (2008). Buckling and Postbuckling Structures: Experimental, Analytical and Numerical Studies. Imperial College London, UK.

Freitas, P. P., Ferreira, R., Cardoso, S., & Cardoso, F. (2007). Magnetoresistive sensors. *Journal of Physics: Condensed Matter*, *19*, 165221.

Ghayesh, M.H., Farajpour, A. (2019). A review on the mechanics of functionally graded nanoscale and microscale structures. *International Journal of Engineering Science*, 137, 8-36.

Ghayesh, M.H., Farokhi, H. (2020) Nonlinear broadband performance of energy harvesters. *International Journal of Engineering Science*, 147, 103202

Gunda, J. B. (2014). Thermal post-buckling & large amplitude free vibration analysis of Timoshenko beams: Simple closed-form solutions. Applied Mathematical Modelling, 38, 4548–4558.

Hamed, M.A., Mohamed, N.A. & Eltaher, M.A. (2020). Stability buckling and bending of nanobeams including cutouts. *Engineering with Computers*, https://doi.org/10.1007/s00366-020-01063-2

Jalaei, M.H., Civalek, Ö. (2019). On dynamic instability of magnetically embedded viscoelastic porous FG nanobeam. *International Journal of Engineering Science*, 143, 14-32.

Ju, Y.-W., Park, J.-H., Jung, H.-R., Cho, S.-J., & Lee, W.-J. (2008). Fabrication and characterization of cobalt ferrite ($CoFe_2O_4$) nanofibers by electrospinning. *Materials Science and Engineering: B*, *147*, 7-12.

Justino, C. I. L., Rocha-Santos, T. A., Duarte, A. C., & Rocha-Santos, T. A. (2010). Review of analytical figures of merit of sensors and biosensors in clinical applications. *TrAC Trends*

MOST WIEDZY Downloaded from mostwiedzy.pl

in Analytical Chemistry, *29*, 1172-1183.

Kabychenkov, A. F., & Lisovskii, F. V. (2019). Flexomagnetic and flexoantiferromagnetic effects in centrosymmetric antiferromagnetic materials. *Technical Physics*, *64*, 980-983.

Karami, B., & Janghorban, M. (2019). On the dynamics of porous nanotubes with variable material properties and variable thickness. *International Journal of Engineering Science*, *136*, 53-66.

Karami, B., & Janghorban, M. (2020). On the mechanics of functionally graded nanoshells. *International Journal of Engineering Science*, *153*, Article 103309.

Karami, B., Janghorban, M., & Rabczuk, T. (2020). Dynamics of two-dimensional functionally graded tapered Timoshenko nanobeam in thermal environment using nonlocal strain gradient theory. *Composites Part B-Engineering*, *182*, 107622.

Li, L., Hu, Y. (2017). Post-buckling analysis of functionally graded nanobeams incorporating nonlocal stress and microstructure-dependent strain gradient effects. *International Journal of Mechanical Sciences*, *120*, 159-170.

Lim, C. W., Zhang, G., & Reddy, J. N. (2015). A Higher-order nonlocal elasticity and strain gradient theory and Its Applications in wave propagation. *Journal of the Mechanics and Physics of Solids*, *78*, 298-313.

Lukashev, P., & Sabirianov, R. F. (2010). Flexomagnetic effect in frustrated triangular magnetic structures. *Physical Review B*, *82*, 094417.

Moosavi, S., Zakaria, S., Chia, C. H., Gan, S., Azahari, N. A., & Kaco, H. (2017). Hydrothermal synthesis, magnetic properties and characterization of $CoFe_2O_4$ nanocrystals. *Ceramics International*, *43*, 7889-7894

Malikan, M., & Eremeyev, V. A. (2020a). Free Vibration of Flexomagnetic Nanostructured Tubes Based on Stress-driven Nonlocal Elasticity. In Analysis of Shells, Plates, and Beams, 1st ed.; Springer Nature, Switzerland, *134*, 215-226.

Malikan, M., & Eremeyev, V. A. (2020b). On the geometrically nonlinear vibration of a piezo-

MOST WIEDZY Downloaded from mostwiedzy.pl

flexomagnetic nanotube. *Mathematical Methods in the Applied Sciences*, https://doi.org/10.1002/mma.6758

Malikan, M., & Eremeyev, V. A. (2020c). On the dynamics of a visco-piezo-flexoelectric nanobeam. *Symmetry*, *12*, 643. doi: 10.3390/sym12040643

Malikan, M., & Eremeyev, V. A. (2020d). Post-critical buckling of truncated conical carbon nanotubes considering surface effects embedding in a nonlinear Winkler substrate using the Rayleigh-Ritz method. *Materials Research Express*, *7*, 025005.

Malikan, M., & Eremeyev, V. A. (2020e). A new hyperbolic-polynomial higher-order elasticity theory for mechanics of thick FGM beams with imperfection in the material composition. *Composite Structures*, *249*, 112486.

Malikan, M., Dimitri, R., & Tornabene, F. (2019). Transient response of oscillated carbon nanotubes with an internal and external damping. *Composites Part B-Engineering*, *158*, 198-205.

Malikan, M., Krasheninnikov, M., & Eremeyev, V. A. (2020). Torsional stability capacity of a nano-composite shell based on a nonlocal strain gradient shell model under a three-dimensional magnetic field. *International Journal of Engineering Science*, *148*, Article 103210.

Malikan, M., Nguyen, V. B., & Tornabene, F. (2018). Damped forced vibration analysis of single-walled carbon nanotubes resting on viscoelastic foundation in thermal environment using nonlocal strain gradient theory. *Engineering Science and Technology, an International Journal*, *21*, 778-786.

Mawassy, N., Reda, H., Ganghoffer, J.-F., Eremeyev, V.A., Lakiss, H. (2020). A variational approach of homogenization of piezoelectric composites towards piezoelectric and flexoelectric effective media. *International Journal of Engineering Science* (submitted)

Pereira, C., Pereira, A. M., Fernandes, C., Rocha, M., Mendes, R., Fernández-García, M. P., Guedes, A., Tavares, P. B., Grenèche, J.-M., Araújo, J. P., & Freire, C. (2012). Superparamagnetic MFe_2O_4 (M = Fe, Co, Mn) Nanoparticles: Tuning the Particle Size and

MOST WIEDZY Downloaded from mostwiedzy.pl

Magnetic Properties through a Novel One-Step Coprecipitation Route. *Chemistry of Materials*, *24*, 1496-1504.

Pan, E., & Han, F. (2005). Exact solution for functionally graded and layered magneto-electro-elastic plates. *International Journal of Engineering Science*, *43*, 321-339.

Pan, E., & Heyliger, P. R. (2003). Exact solutions for magneto-electro-elastic laminates in cylindrical bending. *International Journal of Solids and Structures*, *40*, 6859-6876.

Pradhan, S. C., & Reddy, G. K. (2011). Buckling analysis of single walled carbon nanotube on Winkler foundation using nonlocal elasticity theory and DTM. *Computational Materials Science*, *50*, 1052-1056.

Reddy, J. N. (2010). Nonlocal nonlinear formulations for bending of classical and shear deformation theories of beams and plates. *International Journal of Engineering Science*, *48*, 1507-1518.

Reddy, L. H., Arias, J. L., Nicolas, J., & Couvreur, P. (2012). Magnetic Nanoparticles: Design and Characterization, Toxicity and Biocompatibility, Pharmaceutical and Biomedical Applications. *Chemistry of Materials*, *112*, 5818-5878.

Sahmani, S., & Safaei, B. (2019). Nonlinear free vibrations of bi-directional functionally graded micro/nano-beams including nonlocal stress and microstructural strain gradient size effects. *Thin-Walled Structures*, *140*, 342-356.

Senthil, V. P., Gajendiran, J., Gokul Raj, S., Shanmugavel, T., Ramesh Kumar, G., & Parthasaradhi Reddy, C. (2018). Study of structural and magnetic properties of cobalt ferrite (CoFe2O4) nanostructures. *Chemical Physics Letters*, *695*, 19-23.

Sidhardh, S., & Ray, M. C. (2018). Flexomagnetic response of nanostructures. *Journal of Applied Physics*, *124*, 244101.

Song, X., & Li, S.-R. (2007). Thermal buckling and post-buckling of pinned–fixed Euler–Bernoulli beams on an elastic foundation. *Mechanics Research Communications*, *34*, 164–171.

MOST WIEDZY Downloaded from mostwiedzy.pl

Stevens, K. A., Ricci, R., Davies, G. A. O. (1995). Buckling and postbuckling of composite structures. *Composites*, *26*, 189-199.

Theres Baby, T., & Ramaprabhu, S. (2010). SiO_2 coated Fe_3O_4 magnetic nanoparticle dispersed multiwalled carbon nanotubes based amperometric glucose biosensor. *Talanta*, *80*, 2016-2022.

Timoshenko, S. P., & Gere, J. M. (1989). Theory of elastic stability. 2nd edition. Mineola: Dover.

Wang, C. M., Zhang, Y. Y., Sudha Ramesh, S., & Kitipornchai, S. (2006). Buckling analysis of micro- and nano-rods/tubes based on nonlocal Timoshenko beam theory. *Journal of Physics D: Applied Physics*, *39*, 3904.

Xu, Y., & Wang, E. (2012). Electrochemical biosensors based on magnetic micro/nano particles. *Electrochimica Acta*, *84*, 62-73.

Xin, Y., Fu-bing, X., Hong-wei, L., Feng, W., Di-zhao, C., Zhao-yang, W. (2013). A novel H_2O_2 biosensor based on Fe_3O_4–Au magnetic nanoparticles coated horseradish peroxidase and graphene sheets–Nafion film modified screen-printed carbon electrode. *Electrochimica Acta*, *109*, 750-755.

Zhang, J. X., Zeches, R. J., He, Q., Chu, Y. H., & Ramesh, R. (2012). Nanoscale phase boundaries: a new twist to novel functionalities. *Nanoscale*, *4*, 6196-6204.

Zhang, N., Zheng, Sh., & Chen, D. (2019). Size-dependent static bending of flexomagnetic nanobeams. *Journal of Applied Physics*, *126*, 223901.

Zhou, H., Pei, Y., & Fang, D. (2014). Magnetic field tunable small-scale mechanical properties of nickel single crystals measured by nanoindentation technique. *Scientific Reports*, *4*, 1-6.

MOST WIEDZY Downloaded from mostwiedzy.pl